International Journal of Engineering

Journal Homepage: www.ije.ir

Characterization of Fe₃O₄/rGO Composites from Natural Sources: Application for Dyes Color Degradation in Aqueous Solution

N. Munasir*[a], R. P. Kusumawati[a], D. H. Kusumawati[a], Z. A. I. Supardi[a], A. Taufiq[b], Darminto[c]

[a] Physics Department, Faculty of Mathematics and Natural Science, Universitas Negeri Surabaya, Jl. Ketintang, Surabaya, Indonesia
[b] Physics Department, Faculty of Mathematics and Natural Science, Universitas Negeri Malang, Jl. Surabaya, Malang, Indonesia
[c] Physics Department, Faculty of Science, Institut Teknologi Sepuluh Nopember Surabaya, Jl. A. R Hakim, Sukolilo, Surabaya, Indonesia

ABSTRACT

The magnetite (Fe₃O₄) nanoparticle and graphene oxide (GO) have become interesting materials due to their advanced applications. In this work, we investigated the fabrication of Fe₃O₄ nanoparticles (NPs) from iron sands and reduced graphene oxide (rGO) NPs from natural graphite. The core-shell fabrication of the Fe₃O₄/rGO was conducted by means of ex-situ method using ethanol as the medium. The crystal structure of Fe₃O₄/rGO was observed using X-ray diffraction (XRD) and functional groups were examined using Fourier transform infra-red (FTIR) spectroscopy. The characteristic of the disturbance originated by carbon atoms was investigated by Raman spectroscopy. The morphological, particle sizes and formation studied with transmission electron microscopy (TEM). The magnetic properties were analyzed using vibrating sample magnetometer (VSM). Furthermore, analysis of the adsorption performance, namely: dye-removal efficiency (DRE) and degradation rate (DR), as candidate materials absorbent were performed by means of UV-Vis spectroscopy. The data analysis of structure and phase of Fe₃O₄/rGO presented cubic spinel structure with crystallite size of 26-38 nm. The functional group analysis presented the existence of C-OH, C=O, C-O, and Fe-O. The micrograph analysis from the TEM image showed the particle size of the sample was in the range of 10 - 30 nm. Along with the thickening shell, the saturation magnetization of Fe₃O₄/rGO decreased from 22.60 to 18.48 emu/g and decreased from 29.21 to 10.45 emu/g for Fe₃O₄. Finally, the rGO composition affects the shell wall, which encloses Fe₃O₄ as the core. Interestingly, an increase in absorption characteristic of natural dyes Fe₃O₄/rGO enhanced by the decrease of the shell thickness.

doi: 10.5829/ije.2020.33.01a.03

NOMENCLATURE

GO	*Graphene Oxide*	M	Magnetization (emu/g)
rGO	Reduxed-Graphene Oxide	RE_{MB}	Efficiency of Removal of Mathylene-Blue
DR_{MB}	Degradation Rate of Mathylene-Blue	H_C	Applied Magnetic Field (*Oe*)

1. INTRODUCTION

Raw water pollution is generally due contamination by dissolved substances such as organic matter, heavy metals, microplastics, and so on. These substances come from industrial and household waste, which harms human health. In 2018, 2.1 billion people did not have clean drinking water [1]. This affected their quality of life. At present, 1.9 billion people are living in severe water areas, and their number is expected to increase to 3 billion by 2050. At present, an estimated 1.8 billion people still drink water from water sources contaminated by waste products. Globally, more than 80% of the water resources are polluted by being used for various purposes and returned to the surrounding environment without reprocessing or reuse [1, 2]. Among the multiple criteria for water considered fit for human consumption, is the absence of heavy metal contaminants (Pb, Cu, Cr, As, Ni, Zn, etc.) and organic dyes derived from textile processing. The conventional processing technology

used to remove these contaminants requires expensive equipment and is energy-intensive. In addition, it produces significant quantities of sludge. Therefore, the adsorption process is one of the essential methods for removing metals and natural dyes from water. This method is attracting much attention because it is inexpensive, efficient, and straightforward [3–5].

Recently smart ingredients have been discovered that can filter and purify seawater so that it can be directly drinkable. It has the ability to absorb contaminants in drinking water very well, making it safe for human consumption. The material is graphene (GO), which has a hexagonal chain of carbon chains the size of an atomic order, which has excellent electrical and mechanical properties. It provides new hope for water desalination [6]. Reduction of graphene oxide (GO) can occur by thermal, chemical, or electrochemical methods. GO can be synthesized from graphite, using synthetic media with concentrated sulfuric acid, nitric acid, and potassium permanganate; with the modified Hummers method [7]. There are three stages in the GO production process from graphite. First, the process of graphite oxidation is the formation of graphite oxide from graphite material. Second, the process of slicing the GO layer into one sheet using ultrasonication method. The third, the GO reduction process, whereby reduced graphene (rGO) is formed. In addition, the position of the carbonyl and carboxyl groups on the edge of the sp2 hybridized carbon sheet. These characteristics make the GO very hydrophilic. It produces a stable dispersion consisting mainly of single-layered layers. Recent research shows that rGO has excellent potential as a porous material for seawater desalination-'a rising star' of water purification-which removes various water pollutants such as metallic ions, anions, microplastic, nanoparticles, organic chemicals, and biological substrate [8, 9].

Besides rGO, another new material that is proved to be excellent by research on advanced materials is magnetic nanoparticles (MNPs). MNPs is a kind of nanomaterials that is easily controlled by an external magnetic field. Such material is commonly composed of two components, i.e., magnetic material and its functionalized component. Furthermore, the nanoparticle cluster is constructed by MNPs knowing as nanobeads with the diameter of 50 - 200 nm [10]. As clusters, iron oxides are generally found as maghemite (Fe_2O_3) and magnetite (Fe_3O_4). Fe_3O_4 nanoparticles commonly have particle size smaller than 128 nm with superparamagnetic character providing excellent applications in medical, military, sensors, artificial intelligence, and so forth [10]. The most interesting properties of these particles are their small size, high surface area, and magnetic properties [11]. Among the applications in which these properties of Fe_3O_4 are advantageous is the adsorption of heavy metals (Cr^{-2}, Pb^{+2}, Mn^{+2}, Cu^{+2}, Zn^{+2}, etc.) from water [3, 4] and the removal of dyes [5]. MNPs can be applied thoroughly

in the biomedical field, such as for targeted anticancer drug delivery systems [12], biomedical imaging, and biosensing [13, 14].

At present, many studies utilize this material as the core-shell for creating new materials, for example, with silica to form $Fe_3O_4@SiO_2$ [15], which is useful in drug delivery system (DDS) [16], absorbent for heavy metals [17–20], and natural dyes [18]. In the form of $Fe_3O_4@rGO$ core-shell, it has wide applications such as NOx gas sensors [19], heavy metal absorbents, seawater desalination [21], and so on. For its good electrochemical performance, it is useful in energy storage applications [22] such as in lithium-ion batteries [23]. Fe_3O_4/rGO nanocomposites can be used as photocatalytic material [24, 25], for reducing heavy metals such as Cu^{+2}, Zn^{+2}, Ni^{+2} ions [26], Cr^{-2} [27–30], Pb^{2+} [27, 30], detecting Cd^{+2} [31] ions, degradation of phenol, as an antibacterial [25], for biosensing [31], and as an absorbent for removing dyes in aqueous solutions [32–34]. It has the potential to be used in a sensor to detect the presence of arsenic in mineral water [35, 36], and wastewater treatment [37]. Some methods of synthesis of $Fe_3O_4@rGO$ composites are solvothermal [38], hydrothermal [28, 29], one-pot hydrothermal [27, 39], in-situ hydrothermal [22, 26, 39], in-situ chemical [24], and ex-situ chemical [40]. Each of these methods has its own advantages and, generally, the methods are simple. The usual steps in synthesizing the composite are: first, prepare rGO nanoparticles, then form the Fe_3O_4 nanoparticles together with the process of forming the composite or the core-shell system of Fe_3O_4/rGO. The precursors for the formation of Fe_3O_4 NPs are $FeCl_3.6H_2O$ and $FeCl_2.4H_2O$ with the addition of NH_4OH solution [39].

In the present paper, we report the characterization of Fe_3O_4/rGO composite prepared from natural ingredients and application prospects. Fe_3O_4 NPs was prepared from iron sand, using the co-precipitation method; and rGO nanoparticles were made from natural graphite and then oxidized and reduced by the Hummers method. The formation of core-shell was carried out by ex-situ method. Fe_3O_4/rGO composite characterization was carried out based on its crystal structure, morphology, functional uptake, and magnetic properties. Finally, an analysis of the absorption properties of organic pollutants was carried out using methylene blue.
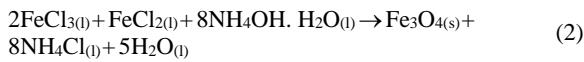
2. EXPERIMENT

2.1. Materials
The materials used in the synthesis of Fe_3O_4 NPs, rGO NPs, and Fe_3O_4/rGO NPs were iron sand (98%), graphite (99%) from coconut shells, HCl (Pro Analysis 37%), NH_4OH, NaOH, H_2O_2, H_2SO_4, $KMnO_4$, $NaNO_3$, ethanol, deionized-water, and several supporting tools. Fe_3O_4/rGO composite material, then prepared by ex-situ method.

2. 2. Synthesis Method

2. 2. 1. Synthesis of Fe₃O₄ Nanoparticle
Fe_3O_4 nanoparticles were prepared from iron sand (98%). In the first stage, 20 grams of iron sand was dissolved in 38 mL HCl and stirred for 10-12 minutes at a temperature of 60 °C. When the color of the sand turned yellow, it was then stopped and cooled to ambient temperature followed by separation with the filtrate. Furthermore, 24 mL NH_4OH was added and stirred to obtain a solid black precipitate. The precipitate was then washed with distilled water and dried in the furnace at 70 °C for 12 h to obtain Fe_3O_4 NPs powder. The chemical reactions that lead to the synthesis of the Fe_3O_4 NPs are as follows [40–42]:

$$Fe_3O_{4(s)} + 8HCl_{(l)} \rightarrow 2FeCl_{(l)} + FeCl_{2(l)} + 4H_2O_{(l)} \qquad (1)$$

$$2FeCl_{3(l)} + FeCl_{2(l)} + 8NH_4OH. H_2O_{(l)} \rightarrow Fe_3O_{4(s)} + 8NH_4Cl_{(l)} + 5H_2O_{(l)} \qquad (2)$$

2. 2. 2. Synthesis of rGO Nanoparticle
The rGO nanoparticles were synthesied from natural graphite obtained from coconut shells burned at a specific temperature, commercially known as activated carbon. In the initial stage, the graphite powder was smoothed and filtered to obtain uniform size particles. Two grams of graphite powder and 1 gram of $NaNO_3$ were mixed in an ice-bath, then 48 mL of H_2SO_4 was added to cause oxidation. Then, 6 grams of $KMnO_4$ was added while stirring; deionized water (~ 290 mL) was also added at a temperature below 90°C. The solution was removed from the heat-bath, and 150 mL of deionized water was added and stirred until the color turned brown. Then, 10 mL of H_2O_2 was added to reduce $KMnO_4$ and stirred for 30 minutes until the solution turned yellow. At this stage, graphite oxide was in a dispersed state in the solution. Then, the solution was washed repeatedly with deionized water to remove the by-products such as salt (till the pH became neutral) and then the solution was filtered. The filtered slurry was dried in an oven in vacuum at 70°C for 12 h, and GO powder thus obtained. 3 grams of GO powder was mixed with 1 mL of deionized water and subjected to the cutting process with ultrasonic vibrations for 2 h at room temperature to obtain GO. Then, hydrazine (80 Wt%) added until the color turned solid black. This stage yielded reduced graphene (rGO). The concentrated precipitate, which was rGO NPs powder, was filtered and dried at 600°C. The steps of the rGO production process are illustrated in Figure 1.
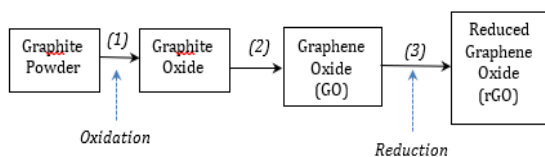

Figure 1. The stages of the process of forming graphite oxide, graphene oxide, and rGO

(1) the oxidation process for the formation of graphite oxides using $NaNO_3$, H_2SO_4, $KMnO_4$, and H_2O_2 as reagents. (2) the stage of grafting the graphite oxide layer to graphene oxide (GO) by the ultrasonication vibration method. Finally (3), the GO reduction process using hydrazine (80% by weight) to obtain rGO.

2. 2. 3. Synthesis of Fe₃O₄/rGO Core-Shell
The shell-core formation process was carried out in conjunction with the process of forming this wrapping skin, in this case, Fe_3O_4 particles were stirred with GO with a one-pot procedure, together with the formation of rGO [27, 43]. Conversely, it could also be prepared by rGO nanoparticles in advance, the shell-forming process, along with the synthesis of Fe_3O_4 nanoparticles followed by procedure discussed by Wang et al. [28]. In this study, NP Fe_3O_4 and rGO were prepared first, then mixed with a specific composition in polar solution, ethanol. The preparation stage consists of mixing all components, namely, Fe_3O_4, rGO, and ethanol using a hot plate magnetic stirrer. The stirring process produced a cell-core slurry. The atomic element of alcohol was released by the drying process to obtain the nanocomposite powders. The prepared samples with mass composition of Fe_3O_4 NPs and rGO varied by 1: 1; 1: 2; 1: 3 and 1: 4 in 10 mL of alcohol.

2. 2. 4. Characterization of Adsorption of Dyes Color in Aqueous Solution
For testing the adsorption of natural dyes by Fe_3O_4/rGO by UV-Visible test, methylene-blue (MB) solution (10 mg/L) was used. The samples for the UV-Visible analysis, namely core-shell samples Fe_3O_4/rGO along with four samples of different composition of Fe_3O_4 and rGO were prepared. Each sample was tested for 2.5 minutes, 5 minutes, and 15 minutes at the room temperature (there were eight samples) for the capacity for adsorption of dye. The adsorption power of the dyes in the UV-Visible test was expressed by the rate of photo degradation (changes in MB concentrations in the solution), then the efficiency of dye removal during the Methylene-Blue degradation process. In the mathematically expressed by Equations (3) and (4), DR_{MB} and RE_{MB} represent "Degradation Rate-MB" "MB-removal efficiency", respectively [23]:

$$DR_{MB} = \frac{c_t}{c_0} \qquad (3)$$

$$ER_{MB} = \left(1 - \frac{c_t}{c_0}\right) \times 100\% \qquad (4)$$

where C_t and C_0 represent the concentration of MB in the solution before and after time t of the adsorption reaction.

2. 3. Characterization
The crystal structure and phase of the elements were analyzed using X-ray diffraction (PAN Analytical, Type: Expert Pro) to detect functional groups in molecular components in materials

by infrared waves using Fourier Transform Infra-Red (Shimadzu, Type: IR Prestige). The magnetic properties of the samples, which were visualized by the hysteresis curve were analyzed using a sample magnetometer vibrating at room temperature (VSM; 7404, Lakeshore, USA). And for D-band and Q-band analysis in rGO and Fe_3O_4/rGO samples, Raman-Shift spectroscopy (Raman Spectrometer, Flashlight R200-785) was used. For dye absorption (the case for MB) UV-Visible spectroscopy (Analytical Jena Specord Plus) was used.

3. RESULT AND DISCUSSION

3. 1. Structure Analysis of Fe₃O₄@rGO NPs

X-ray diffraction patterns of Fe_3O_4 nanoparticles, Fe_3O_4/rGO, and core-shell Fe_3O_4/rGO are presented in Figure 2. The details, including the 2 theta angles and the (hkl) planes are shown in Table 1. In the highest peak field (311), the crystal sizes were analyzed for each sample using the Debye Scherrer (D) formula, and were observed to be 26.32, 37.59, and 37.51 nm, respectively. For Fe_3O_4/rGO samples with Fe_3O_4: rGO ratios of 1: 1, 1: 2, and 1: 3. If the diffraction results of each sample were analyzed, except at 2θ of 5° and 18°, there was no other peak, which indicates a particular crystal field (e.g., 001, belongs to GO) [24], which signifies all the phase formed is rGO. The crystalline areas of each Fe_3O_4/rGO sample, indicate that the crystal plane belonging to the Fe_3O_4 NPs (Figure 2) matches the JCPDS database, 65-3107, and shows results that are comparable with the results reported by previous studies [10, 40, 42, 44, 45]. The increase of rGO composition in the composites did not change the crystal structure. However, it changed the particle size of the composites in forming superparamagnetic chain in graphene net.

3. 2. Functional Groups of Fe₃O₄/rGO NPs

FTIR is a technique used for obtaining an infrared spectrum of absorption in solid, liquid, and gas materials. Adsorptions of Fe_3O_4, rGO and Fe_3O_4/rGO samples in
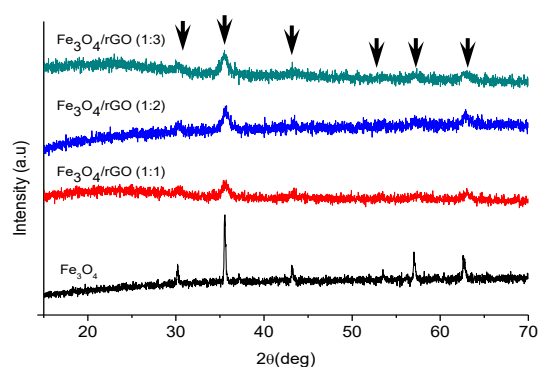
TABLE 1. Pattern X-ray of Fe_3O_4@rGO Nanocomposite

Peak (2 theta), samples of Composites (Fe_3O_4:rGO)			(hkl)	Average Crystallite Sizes (Debye Scherrer) $D =(0.9\lambda/\beta \cos\theta)$ at planes (311), (nm)			Ref.
1:1	1:2	1:3					
30.42°	30.34°	30.17°	(220)				
35.62°	35.61°	35.45°	(311)	26.32	37.59	37.51	[23] [45]
43.37°	43.47°	43.51°	(400)				[46]
53.69°	53.71°	53.74°	(422)				[41, 44] [23, 39]
57.42°	57.46°	57.48°	(511)				[43]
62.98°	62.87°	62.64°	(440)				[47]

the infrared wave areas are presented in Table 2, and shown in Figures 3 and 4. Range of vibrations in Fe-O bonds that indicate the presence of iron oxide (Fe^{2+}) is 470 cm^{-1}-580 cm^{-1}. Stretching of C-O aromatic groups or epoxide groups is shown by a stretch of vibrations that occur in the area of 1070 cm^{-1} and 1176 cm^{-1} [48]. In the C=C group the aromatic stretch alkene group was identified to occur at 1660 cm^{-1} and the carboxyl stretch C=O, recorded in the area of 1726 cm^{-1}. The presence of the H_2O (%) transmittance function group on Fe_3O_4/rGO was smaller than Fe_3O_4, and the rGO was stretching vibration in the O-H bond group identified at 3450 cm^{-1}.

The same analysis was applied to other functional groups, C-O and C=O bond groups, whose vibrations are smaller as compared to rGO materials. This condition indicates the presence of Fe^{2+} and Fe^{3+} ions from Fe_3O_4 and would weaken the vibration of the bonding of carbon atoms [44, 47, 49]. The presence of Fe^{2+} ions as a reducing agent is an essential factor in the redox reaction of Fe_3O_4/rGO formation. The presence of Fe-O functional groups is evidence of Fe_3O_4 that has successfully entered into the Fe_3O_4/rGO nano-composite system. The presence of functional groups C-O and C=O is the evidence that the system has characteristics of

Figure 2. Pattern of XRD of Fe_3O_4/rGO (1:1); Fe_3O_4/rGO (1:2), and Fe_3O_4/rGO (1:3)

TABLE 2. FTIR of Fe_3O_4@rGO Nanocomposite

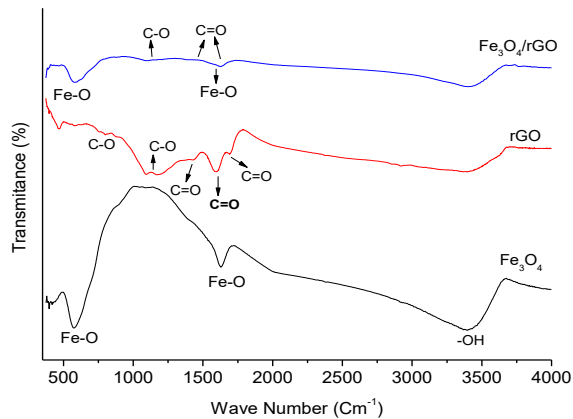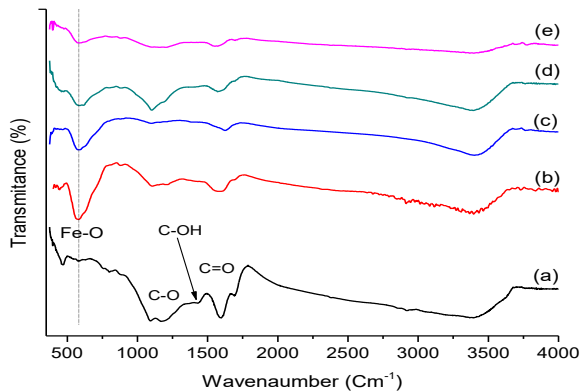| Wave Number of Samples (cm^{-1})	Functional Group	Wavenumbers from Reference (cm^{-1})	Ref.
470 and 580	Fe-O	527, 578	[43]
1070 1176	Epoxy group Stretching C-O	1061, 1073, 1178	[46]
1660	Aromatic stretching C=C	1625,1724	[48]
1726	Carboxyl-stretching C=O	1723,1730	[46]
3450	Stretching vibration of O-H bonding	2900-3600	[41, 44]

Figure 3. FTIR of: Fe_3O_4, rGO, and Fe_3O_4/rGO

Figure 4. FTIR of rGO (a) and Fe_3O_4/rGO samples: 1:1(b), 1:2(c), 1:3(d) dan 1:4(e)

graphene and reduced graphene oxide. There are two extreme peaks, namely, at 580 cm^{-1} (Fe-O bonding) and 1726 cm^{-1} (C=O) (see Figures 3 and. 4), which indicates that there are two core-shell constituents, namely Fe_3O_4 NPs and rGO NPs.

3. 3. Raman Spectroscopy of Fe_3O_4/rGO NPs
Raman spectroscopy is an excellent tool for investigating the ordered and disordered crystal structures of carbonaceous materials such as GO, rGO, and Fe_3O_4/rGO. The D-band peak (~1,380.0 cm^{-1}) and the G-band peak (1,588.5 cm^{-1}) are shown in Figure 5. In rGO and (~1,379.5 cm^{-1}) and G-band (1,586 cm^{-1}) of Fe_3O_4/rGO samples, there is a slight leftward shift. In both rGO and in the core-shell, the intensity, and ratio of D-band and G-band changed. In rGO, the ratio of D-band and G-band intensity was I_D/I_G=0.80, and in core-shell, the intensity was I_D/I_G=0.91. D-band indicates that there is sp^3-site vibration. Defects in the GO field and the G-band indicate that there is a vibration of sp^2 carbon atoms in the hexagonal 2-D lattice of rGO and GO. The position and intensity of D and G bands greatly influenced the transformation of the structure of carbonaceous material

[23]. Decreased intensity and shift in the position of D-band and G-band Fe_3O_4/rGO from rGO (Shift-Raman spectra), presumably due to the presence of Fe_3O_4 nanoparticles scattered in rGO carbon polymer networks [24, 49].

In previous studies, there were slight changes in position from the peak D-band and G-band, to rGO (D-band 1324 cm^{-1} and G-band 1573 cm^{-1}), I_D/I_G=1.84 [49], and GO (D-band ~1,350 and G-band ~1,580), and indicated an increase in defects if the I_D/I_G ratio <1 means small imperfections [24]. Based on the previous work [50], it was found that the displacement of peak position of peak-D and peak-G for Raman-spectroscopy of rGO, occurred i.e, from 1353.20 cm^{-1} to 1380.0 cm^{-1} and from 1586.56 cm^{-1} to 1588.50 cm^{-1}, respectively. Addition of Fe_3O_4 content into rGO influenced in reducing peak intensity of peak-G and peak-D. It corresponds that the Fe_3O_4 particles place C-chains position in the broken rGO. Moreover, the presence of Fe_3O_4 particles in the Fe_3O_4/rGO composites also changed the position of peak-D and peak-G to the lower position. The small difference of intensities for rGO and Fe_3O_4/rGO represented the disorder level of C bound.

3. 4. Magnetic Properties by VSM of Fe_3O_4/rGO Nanoparticles   The Fe_3O_4 NPs are soft-magnetic materials (Figures 6(a) and 6(b)), which is indicated by the narrow hysteresis curve area (Figure 6(a)). Even when wrapped with rGO as a core-shell, it is still soft-magnetic [39], but its strong magnetization has dropped dramatically. Iron is a type of paramagnetic material, where the magnetization is positive (<10^5 order); and this magnetite material is a superparamagnetic type [51]. According to the previous work [45], it is also found that the Fe_3O_4 nanoparticles with the particle size of 1-100 nm presented as a superparamagnetic material.

The value of magnetic susceptibility or saturation magnetization of each Fe_3O_4/rGO sample is strongly influenced by the large composition of Fe_3O_4 NPs
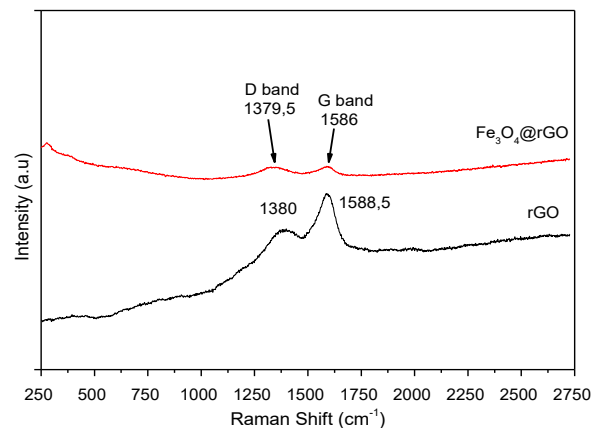

Figure 5. Raman shift of rGO and Fe_3O_4/rGO

(a)

(b)

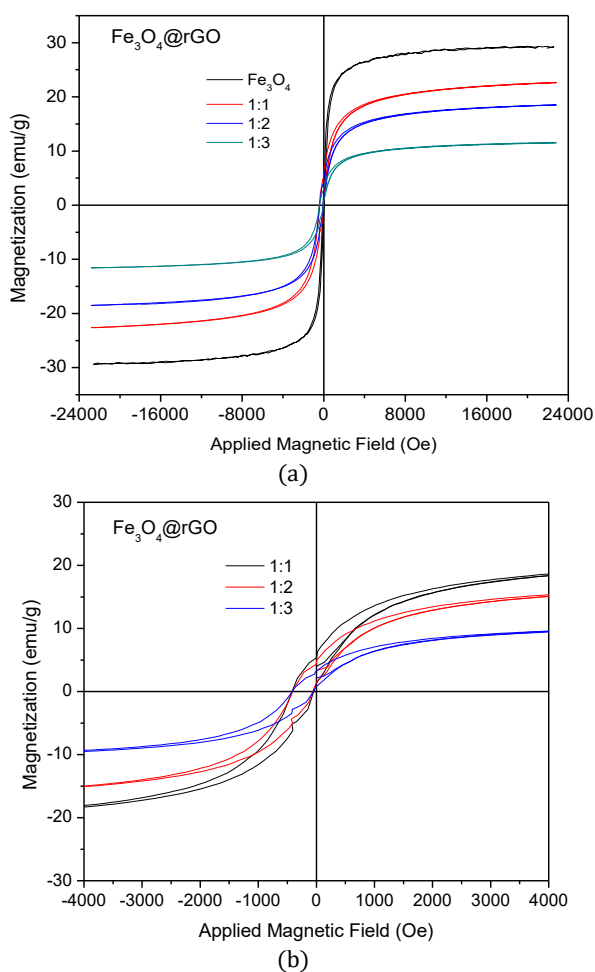**Figure 6.** (a) Curve of hysteresis of Fe_3O_4-NPs and Fe_3O_4/rGO: 1:1; 1:2; and 1:3; (b). Curve of hysteresis of Fe_3O_4/rGO for variation composition

as the cell nucleus and rGO as the cell skin that coats. The less presence of rGO, the thinner the skin, so that superparamagnetic saturation is stronger, as shown in Figure 6(a). Each Fe_3O_4/rGO sample showed different saturation magnetization (Ms) and different remanence saturation magnets. That is: 29.21 emu/g and 6.2 emu/g, 22.60 emu/g and 4.56 emu/g, 18.48 emu/g and 3.91 emu/g and 3.91 emu/g, and 10.45 emu/g, and 10.45 emu/g and 3.23 emu/g; with a composition of 1: 1, 1: 2, and 1: 3.

The coercive magnetic field is very small for each sample (<100 Oe) (see Figure 6 (b)). At composition 1:1, the magnetization saturation of Fe_3O_4 NPs can reduce by 22.63%. For Fe_3O_4/rGO (1:2) sample, the reduction is 36.73%, and for Fe_3O_4/rGO (1:3) it falls by 64.22% (more than half the saturation of magnetization of Fe_3O_4 NPs). These superparamagnetic properties, which play a role in the application of natural dye absorption, absorption of heavy metals and other applications [25, 28, 33, 52] will be presented in the following section.

3. 5. Morphology of Fe_3O_4/rGO Nanoparticles
Characterization of powder materials using transmission electron microscope (TEM) is very important to determine the morphological profile and size of the constituent particles of the core-shell. In Figure 7, the morphology of Fe_3O_4/rGO (for compositions 1: 3). It appears that the shape of particles tend to be round and form agglomerations with particle sizes around 10-30 nm; according to the estimated crystal size calculated by the Debye Scherrer approach (~26 - 38 nm). The Fe_3O_4 particles in Figure 6 are confirmed to appear as balls (black) located between the rGO particles, which appear to be more dominant as nets containing superparamagnetic particles Fe_3O_4. The rGO particles exceed Fe_3O_4 particles by more than three times, so they act more as a matrix or coating that wrap around the magnetite particle cores [25].

3. 6. UV-Vis Properties of Fe_3O_4/rGO Nanoparticles
The adsorption activity of the Fe_3O_4/rGO material was observed by monitoring the MB color change under irradiation of visible light ($\lambda \geq 420$ nm). Large concentrations of MB solution were analyzed by measuring the peak wavelength intensity in the range of 240-800 nm UV-visible spectroscopic graph. Look at the spectrum of Figure 8 of UV-Vis, specifically for MB in water. The adsorption peak for the MB solution (Figure 8 (a)) is very high at positions: 660 nm, 300 nm,
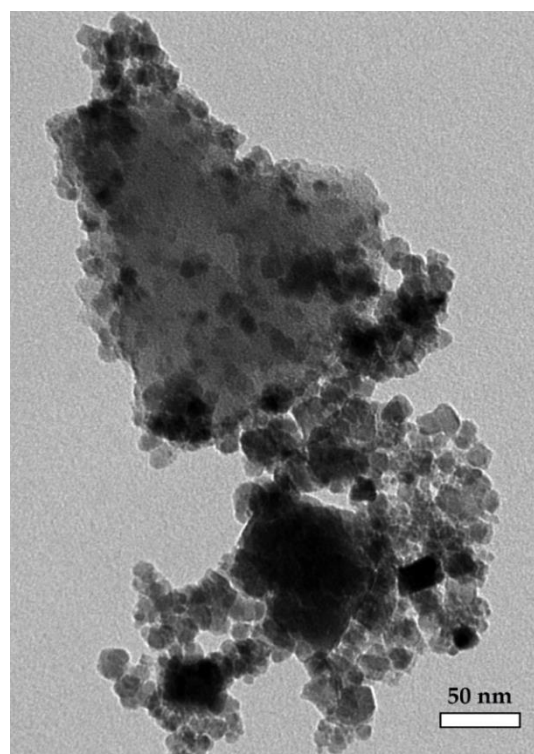

Figure 7. TEM Micrograph of magnetite Fe_3O_4@rGO Nanocomposite (#1:3)

and 240 nm. The adsorption peak for the MB solution (Figure 8 (a)) is very high at positions: 660 nm, 300 nm, and 240 nm. As for the MB solution that has been absorbed by Fe_3O_4/rGO particles has decreased dramatically. Each sample shows a different peak height of the adsorption. The lower presence of RGO in the composition of NP Fe_3O_4 has MB-dye absorption in a stronger solution, and vice versa (Figure 8 (b-e)). Examples of absorption duration (2.5-20 minutes) also affect adsorption. The longer the absorption time, the higher the MB degradation in water. Therefore, for nanocomposite samples with a composition of 1: 1 between rGO and Fe_3O_4 has the highest MB degradation rate. In the core-shell system, the formation of rGO particles which is less than Fe_3O_4 marks the thinness of the shell in the system, so that the magnetic properties are stronger. Similarly, with an increase in the number of rGO particle compositions, the thickness of the shell increases, so the magnetic properties decrease.

The degradation activity of Fe_3O_4/rGO core-shell investigated with the degradation of a model of organic dye pollutants, namely, methylene blue (MB The results of the degradation study of Fe_3O_4/rGO materials on MB solution). are shown in Figure 9. During the adsorption process by Fe_3O_4/SiO_2 in MB solution, for the first 2.5 minutes, the absorption of MB was drastic (96.47%, 95.38%, and 86.62%, respectively for each sample). After that, in the next 5 minutes, MB removal increased by 3.62%, 4.75%, and 14.49%, and after the next 15 minutes, the MB removal was maximal. The composition of Fe_3O_4 and rGO (#1:1, #1:2, and #1:3) also influenced dye-removal efficiency (DRE) and degradation rate (DR) as shown in Figures10 and 11 [23, 40].

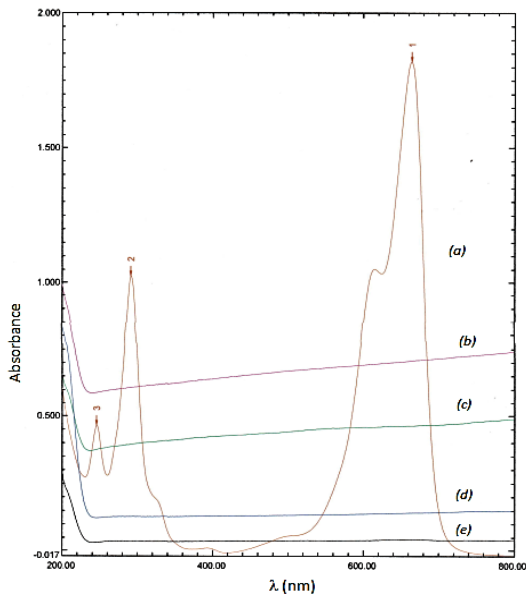**Figure 8.** UV-Vis Spectra of: (a) MB and (b-e) MB/Fe3O4/rGO (#1:4, #1:3, #1:2 and #1:1) after 2.5 min

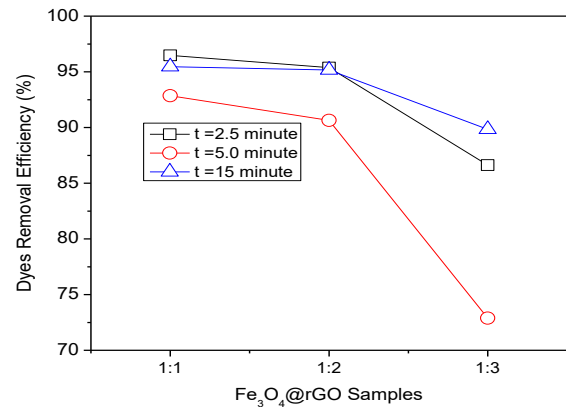**Figure 9.** Degradation of Methylene-Blue by Fe_3O_4@rGO (#1:1) (example)

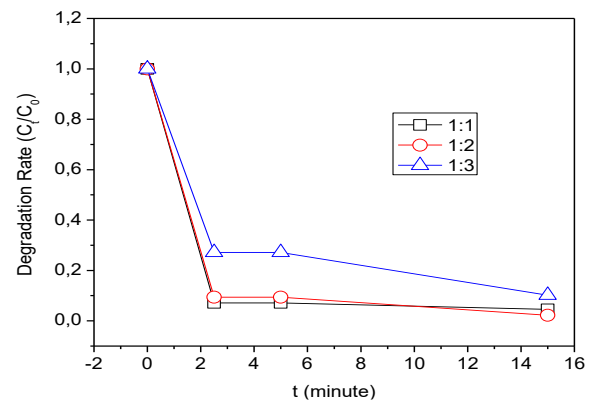**Figure 10.** Dyes Removal Efficiency (DRE_{MB}) by Fe_3O_4@rGO Core-shell

Figure 11. Degradation Rate (C_t/C_0) of Fe_3O_4@rGO Samples

The absorptivity for dyes in each sample showed a trend that the higher the composition of rGO, the thicker the shell and the lesser effect of dyes removal efficiency (%). Also, as the adsorption process increases, there is a dramatic reduction in the impact of dye removal efficiency. It is due to the maximum effective adsorption process that has occurred in the first 2.5 minutes; this applies to all types of samples (Figure 9). Results for the decreased MB decolorization rate, for each sample, shows a downward trend. The decline was drastic, in the

MB removal process in the initial stages (2.5 minutes) and was very useful. However, not all MB was absorbed so that for the next time, the MB removal process still occurred. Degradation of organic dyes (such as methylene blue) by magnetic particles Fe_3O_4@rGO is more effective and more straightforward than WO_3/ TiO_2 particles whose photocatalyst principle works under ultraviolet-visible [53].

4. CONCLOUSION

The Fe_3O_4/rGO composite was successfully fabricated from environmentally friendly iron sand and activated carbon materials, and the method used was quite simple (ex-situ). The crystal field, crystal size, and magnetite phase, and the stretching function groups of carbon (C-OH, C-O, and C=O) and Fe-O as indicators have produced Fe_3O_4/rGO. D-band and G-band are characteristics of rGO analyzed by Raman spectroscopy. In rGO, the ratio of D-band and G-band intensity is I_D/I_G = 0.80 while in the Fe_3O_4/rGO composite, the intensity ratio is I_D/I_G = 0.91, there is a shift. The magnetic properties of Fe_3O_4 and its composite were analyzed using VSM, and superparamagnetic characteristics. The presence of rGO as a shell affected the value of composite magnetization. The formation, particle size, and composite morphology can be displayed using the TEM analysis. The superparamagnetic properties of Fe_3O_4/rGO were then applied to the adsorption of dyes colors, as in the MB observed with the ultraviolet-visible.

5. ACKNOWLEDGMENTS

6. REFERENCES

1. Vose, J. M., "Forest and Water in the 21st Century: A Global Perspective", *Journal of Forestry*, Vol. 117, No. 1, (2019), 80–85.

2. Cohen-Shacham, E., Walters, G., Janzen, C. and Maginnis, S., Nature-based solutions to address global societal challenges, IUCN International Union for Conservation of Nature, (2016).

3. Boretti, A., Al-Zubaidy, S., Vaclavikova, M., Al-Abri, M., Castelletto, S. and Mikhalovsky, S., "Outlook for graphene-based desalination membranes", *NPJ Clean Water*, Vol. 1, No. 1, (2018), 1–11.

4. Song, J., Wang, X. and Chang, C. T., "Preparation and characterization of graphene oxide", *Journal of Nanomaterials*, Vol. 2014, (2014), 1–6.

5. Gandhi, M.R., Vasudevan, S., Shibayama, A. and Yamada, M., "Graphene and graphene-based composites: A rising star in water purification-a comprehensive overview", *ChemistrySelect*, Vol. 1, No. 15, (2016), 4358–4385.

6. Wang, Z., Wu, A., Colombi Ciacchi, L. and Wei, G., "Recent advances in nanoporous membranes for water purification", *Nanomaterials*, Vol. 8, No. 65, (2018), 1–19.

7. Köseoglu, Y. and Kavas, H., "Size and surface effects on magnetic properties of Fe3O4 nanoparticles", *Journal of Nanoscience and Nanotechnology*, Vol. 8, No. 2, (2008), 584–590.

8. Aftabtalab, A. and Sadabadi, H., "Application of magnetite (Fe3O4) nanoparticles in hexavalent chromium adsorption from aquatic solutions", *Journal of Petroleum & Environmental Biotechnology*, Vol. 6, No. 200, (2015), 1–6.

9. Giraldo, L., Erto, A. and Moreno-Piraján, J. C., "Magnetite nanoparticles for removal of heavy metals from aqueous solutions: synthesis and characterization", *Adsorption*, Vol. 19, No. 2–4, (2013), 465–474.

10. Mishra, A. and Mohanty, T., "Structural and morphological study of magnetic Fe3O4/reduced graphene oxide nanocomposites", *Materials Today: Proceedings*, Vol. 3, No. 6, (2016), 1576–1581.

11. Sivashankar, R., Sathya, A.B., Vasantharaj, K. and Sivasubramanian, V., "Magnetic composite an environmental super adsorbent for dye sequestration–A review", *Environmental Nanotechnology, Monitoring & Management*, Vol. 1, (2014), 36–49.

12. Yew, Y.P., Shameli, K., Miyake, M., Khairudin, N.B.B.A., Mohamad, S.E.B., Naiki, T. and Lee, K. X., "Green biosynthesis of superparamagnetic magnetite Fe3O4 nanoparticles and biomedical applications in targeted anticancer drug delivery system: A review", *Arabian Journal of Chemistry*, Vol. 13, No. 1, (2018), 2287–2308.

13. Mamani, J.B., Gamarra, L.F. and Brito, G. E. D. S., "Synthesis and characterization of Fe3O4 nanoparticles with perspectives in biomedical applications", *Materials Research*, Vol. 17, No. 3, (2014), 542–549.

14. Gee, S.H., Hong, Y.K., Erickson, D.W., Park, M.H. and Sur, J. C., "Synthesis and aging effect of spherical magnetite (Fe 3 O 4) nanoparticles for biosensor applications", *Journal of Applied Physics*, Vol. 93, No. 10, (2003), 7560–7562.

15. Ding, H.L., Zhang, Y.X., Wang, S., Xu, J.M., Xu, S.C. and Li, G. H., "Fe3O4@ SiO2 core/shell nanoparticles: the silica coating regulations with a single core for different core sizes and shell thicknesses", *Chemistry of Materials*, Vol. 24, No. 23, (2012), 4572–4580.

16. Abbas, M., Torati, S.R., Lee, C.S., Rinaldi, C. and Kim, C. G., "Fe3O4/SiO2 core/shell nanocubes: novel coating approach with tunable silica thickness and enhancement in stability and biocompatibility", *Journal of Nanomedicine and Nanotechnology*, Vol. 5, No. 6, (2014), 1–8.

17. Majeed, J., Ramkumar, J., Chandramouleeswaran, S. and Tyagi, A. K., "Fe3O4@ SiO2 core-shell nanoparticles: Synthesis, characterization and application in environmental remediation", In American Institute of Physics Conference Series (Vol. 1591), (2014), 605–607.

18. Subhan, F., Aslam, S., Yan, Z., Khan, M., Etim, U.J. and Naeem, M., "Effective adsorptive performance of Fe 3 O 4@ SiO 2 core shell spheres for methylene blue: kinetics, isotherm and mechanism", *Journal of Porous Materials*, Vol. 26, No. 5, (2019), 1465–1474.

19. Yang, Y., Sun, L., Dong, X., Yu, H., Wang, T., Wang, J., Wang, R., Yu, W. and Liu, G., "Fe3O4/rGO nanocomposite: synthesis and enhanced NO x gas-sensing properties at room temperature", *RSC Advances*, Vol. 6, No. 43, (2016), 37085–37092.

20. Hoan, V., Thi, N., Thu, A., Thi, N., Duc, H.V., Cuong, N.D., Quang Khieu, D. and Vo, V., "Fe3O4/reduced graphene oxide nanocomposite: synthesis and its application for toxic metal ion removal", *Journal of Chemistry*, Vol. 2016, (2016), 1–10.

21. Narayanan, T.N., Liu, Z., Lakshmy, P.R., Gao, W., Nagaoka, Y., Kumar, D.S., Lou, J., Vajtai, R. and Ajayan, P. M., "Synthesis of reduced graphene oxide–Fe3O4 multifunctional freestanding membranes and their temperature dependent electronic transport properties", *Carbon*, Vol. 50, No. 3, (2012), 1338–1345.

22. Saha, S., Jana, M., Samanta, P., Murmu, N.C., Kim, N.H., Kuila, T. and Lee, J. H., "Hydrothermal synthesis of Fe3O4/RGO composites and investigation of electrochemical performances for energy storage applications", *RSC Advances*, Vol. 4, No. 84, (2014), 44777–44785.

23. Zhao, Q., Liu, J., Wang, Y., Tian, W., Liu, J., Zang, J., Ning, H., Yang, C. and Wu, M., "Novel in-situ redox synthesis of Fe3O4/rGO composites with superior electrochemical performance for lithium-ion batteries", *Electrochimica Acta*, Vol. 262, (2018), 233–240.

24. Peik-See, T., Pandikumar, A., Ngee, L.H., Ming, H.N. and Hua, C. C., "Magnetically separable reduced graphene oxide/iron oxide nanocomposite materials for environmental remediation", *Catalysis Science & Technology*, Vol. 4, No. 12, (2014), 4396–4405.

25. Padhi, D.K., Panigrahi, T.K., Parida, K., Singh, S.K. and Mishra, P. M., "Green synthesis of Fe3O4/RGO nanocomposite with enhanced photocatalytic performance for Cr (VI) reduction, phenol degradation, and antibacterial activity", *ACS Sustainable Chemistry & Engineering*, Vol. 5, No. 11, (2017), 10551–10562.

26. Moradinasab, S. and Behzad, M., "Removal of heavy metals from aqueous solution using Fe3O4 nanoparticles coated with Schiff base ligand", *Desalination and Water Treatment*, Vol. 57, No. 9, (2016), 4028–4036.

27. Cao, W., Ma, Y., Zhou, W. and Guo, L., "One-pot hydrothermal synthesis of rGO-Fe3O4 hybrid nanocomposite for removal of Pb (II) via magnetic separation", *Chemical Research in Chinese Universities*, Vol. 31, No. 4, (2015), 508–513.

28. Wang, H., Yuan, X., Wu, Y., Chen, X., Leng, L., Wang, H., Li, H. and Zeng, G., "Facile synthesis of polypyrrole decorated reduced graphene oxide–Fe3O4 magnetic composites and its application for the Cr (VI) removal", *Chemical Engineering Journal*, Vol. 262, (2015), 597–606.

29. Sun, Y.F., Chen, W.K., Li, W.J., Jiang, T.J., Liu, J.H. and Liu, Z. G., "Selective detection toward Cd2+ using Fe3O4/RGO nanoparticle modified glassy carbon electrode", *Journal of Electroanalytical Chemistry*, Vol. 714, (2014), 97–102.

30. Al-Farhan, B. S., "Removal of Cd and Pb Ions from Aqueous Solutions Using Bentonite-Modified Magnetic Nanoparticles", *International Journal of Nano Dimension*, Vol. 2, No. 1, (2016), 27–31.

31. Yu, L., Wu, H., Wu, B., Wang, Z., Cao, H., Fu, C. and Jia, N., "Magnetic Fe3O4-reduced graphene oxide nanocomposites-based electrochemical biosensing", *Nano-Micro Letters*, Vol. 6, No. 3, (2014), 258–267.

32. Yang, S., Zeng, T., Li, Y., Liu, J., Chen, Q., Zhou, J., Ye, Y. and Tang, B., "Preparation of graphene oxide decorated Fe3O4@SiO2 nanocomposites with superior adsorption capacity and SERS detection for organic dyes", *Journal of Nanomaterials*, Vol. 16, No. 1, (2015), 1–8.

33. Yang, L., Tian, J., Meng, J., Zhao, R., Li, C., Ma, J. and Jin, T., "Modification and characterization of Fe3O4 nanoparticles for use in adsorption of alkaloids", *Molecules*, Vol. 23, No. 3, (2018), 176–185.

34. Namvari, M. and Namazi, H., "Clicking graphene oxide and Fe3O4 nanoparticles together: an efficient adsorbent to remove dyes from aqueous solutions", *International Journal of*

Environmental Science and Technology, Vol. 11, No. 6, (2014), 1527–1536.

35. Cui, H., Yang, W., Li, X., Zhao, H. and Yuan, Z., "An electrochemical sensor based on a magnetic Fe3O4 nanoparticles and gold nanoparticles modified electrode for sensitive determination of trace amounts of arsenic (III)", *Analytical Methods*, Vol. 4, No. 12, (2012), 4176–4181.

36. Chimezie, A.B., Hajian, R., Yusof, N.A., Woi, P.M. and Shams, N., "Fabrication of reduced graphene oxide-magnetic nanocomposite (rGO-Fe3O4) as an electrochemical sensor for trace determination of As (III) in water resources", *Journal of Electroanalytical Chemistry*, Vol. 796, (2017), 33–42.

37. Mahalingam, S. and Ahn, Y. H., "Improved visible light photocatalytic activity of rGO–Fe3O4–NiO hybrid nanocomposites synthesized by in situ facile method for industrial wastewater treatment applications", *New Journal of Chemistry*, Vol. 42, No. 6, (2018), 4372–4383.

38. Liu, Y.W., Guan, M.X., Feng, L., Deng, S.L., Bao, J.F., Xie, S.Y., Chen, Z., Huang, R.B. and Zheng, L. S., "Facile and straightforward synthesis of superparamagnetic reduced graphene oxide–Fe3O4 hybrid composite by a solvothermal reaction", *Nanotechnology*, Vol. 24, No. 2, (2012), 1–10.

39. Wang, Q., Zhang, X., Huang, L., Zhang, Z. and Dong, S., "One-pot synthesis of Fe3O4 nanoparticle loaded 3D porous graphene nanocomposites with enhanced nanozyme activity for glucose detection", *ACS applied materials & interfaces*, Vol. 9, No. 8, (2017), 7465–7471.

40. Kusumawati, R. P., "Synthesis and Characterization of Fe3O4@ rGO Composite with Wet-Mixing (ex-situ) Process", *Journal of Physics: Conference Series*, Vol. 1171, No. 1, (2019), 1–5.

41. Rahmawati, R., Taufiq, A., Sunaryono, S., Fuad, A., Yuliarto, B., Suyatman, S. and Kurniadi, D., "Synthesis of magnetite (Fe3O4) nanoparticles from iron sands by coprecipitation-ultrasonic irradiation methods", *Journal of Materials and Environmental Science*, Vol. 9, (2018), 155–160.

42. Dewanto, A.S., Kusumawati, D.H., Dewanto, A.S., Kusumawati, D.H., Putri, N.P., Yulianingsih, A., Sa'adah, I.K.F., Taufiq, A., Hidayat, N., Sunaryono, S. and Supardi, Z.A.I.Putri, N.P., Yulianingsih, A., Sa'adah, I.K.F., Taufiq, A., Hidayat, N., Sunaryono, Z. A. I., "Structure Analysis of Fe3O4@ SiO2 Core Shells Prepared from Amorphous and Crystalline SiO2 Particles", In IOP Conference Series: Materials Science and Engineering (Vol. 367), (2018), 1–8.

43. Zhu, M. and Diao, G., "Synthesis of porous Fe3O4 nanospheres and its application for the catalytic degradation of xylenol orange", *The Journal of Physical Chemistry C*, Vol. 115, No. 39, (2011), 18923–18934.

44. Rezapour, M., "One-step Electrochemical Synthesis and Characterization of High Performance Magnetite/reduced Graphene Oxide Nanocomposite", *Analytical & Bioanalytical Electrochemistry*, Vol. 10, No. 4, (2018), 450–464.

45. Dewanto, A.S., Yulianingsih, A., Saadah, I.K.F., Supardi, Z.A.I., Mufid, A. and Taufiq, A., "Composites of Fe3O4/SiO2 from Natural Material Synthesized by Co-Precipitation Method", In IOP Conference Series: Materials Science and Engineering (Vol. 202), (2017), 1–6.

46. Zhu, S., Guo, J., Dong, J., Cui, Z., Lu, T., Zhu, C., Zhang, D. and Ma, J., "Sonochemical fabrication of Fe3O4 nanoparticles on reduced graphene oxide for biosensors", *Ultrasonics Sonochemistry*, Vol. 20, No. 3, (2013), 872–880.

47. Kamakshi, T., Sundari, G.S., Erothu, H. and Rao, T. P., "Synthesis and characterization of graphene based iron oxide (Fe3O4) nanocomposites", *Rasayan Journal of Chemistry*, Vol. 11, No. 3, (2018), 1113–1119.

48. Kaminska, B., Kaczmarek, L., Larocque, S. and Chaudhuri, A., "Activity-dependent regulation of cytochrome b gene expression

in monkey visual cortex", *Journal of Comparative Neurology*, Vol. 379, No. 2, (1997), 271–282.

49. Sharma, N., Sharma, V., Jain, Y., Kumari, M., Gupta, R., Sharma, S.K. and Sachdev, K., "Synthesis and characterization of graphene oxide (GO) and reduced graphene oxide (rGO) for gas sensing application", *Macromolecular Symposia*, Vol. 376, No. 1, (2017), 1–5.

50. Hidayah, N.M.S., Liu, W.W., Lai, C.W., Noriman, N.Z., Khe, C.S., Hashim, U. and Lee, H. C., "Comparison on graphite, graphene oxide and reduced graphene oxide: Synthesis and characterization", In AIP Conference Proceedings: Materials Science and Engineering (Vol. 1892), (2017), 1–8.

51. James, R. D., "Materials science: Magnetic alloys break the rules", *Nature*, Vol. 521, No. 7552, (2015), 298–299.

52. Sun, H., Zeng, X., Liu, M., Elingarami, S., Li, G., Shen, B. and He, N., "Synthesis of size-controlled Fe3O4@SiO2 magnetic nanoparticles for nucleic acid analysis", *Journal of Nanoscience and Nanotechnology*, Vol. 12, No. 1, (2012), 267–273.

53. Wahyuono, R., Ernawati, L., Maharsih, I.K., Widiastuti, N. and Widiyandari, H., "Mesoporous WO3/TiO2 Nanocomposites Photocatalyst for Rapid Degradation of Methylene Blue in Aqueous Medium", *International Journal of Engineering - Transaction A: Basics*, Vol. 32, No. 10, (2019), 1345–1352.

Characterization of Fe₃O₄/rGO Composites from Natural Sources: Application for Dyes Color Degradation in Aqueous Solution

N. Munasir[a], R. P. Kusumawati[a], D. H. Kusumawati[a], Z. A. I. Supardi[a], A. Taufiq[b], Darminto[c]

[a] *Physics Department, Faculty of Mathematics and Natural Science, Universitas Negeri Surabaya, Jl. Ketintang, Surabaya, Indonesia*
[b] *Physics Department, Faculty of Mathematics and Natural Science, Universitas Negeri Malang, Jl. Surabaya, Malang, Indonesia*
[c] *Physics Department, Faculty of Science, Institut Teknologi Sepuluh Nopember Surabaya, Jl. A. R Hakim, Sukolilo, Surabaya, Indonesia*

چکیده

نانوذرات مگنتیت (Fe₃O₄) و اکسید گرافن (GO) به دلیل کاربردهای پیشرفته‌شان به مواد جالبی تبدیل شده‌اند. در این پژوهش، تولید نانوذرات (NPs) Fe₃O₄ از ماسه‌های آهنی و کاهش اکسید گرافن (rGO) نانوذرات از گرافیت طبیعی را بررسی کردیم. ساخت هسته–پوسته rGO / Fe₃O₄ با استفاده از روش خارج از محل در محیط اتانول انجام شد. ساختار بلوری rGO / Fe₃O₄ با استفاده از پراش پرتو X (XRD) مشاهده شد و گروه‌های عملکردی با استفاده از طیف‌سنجی تبدیل فوریه (FTIR) فروسرخ مورد بررسی قرار گرفتند. ویژگی اختلال ناشی از اتم‌های کربن توسط طیف سنجی رامان بررسی شد. مورفولوژی، اندازه‌ی ذرات و شکل‌گیری با میکروسکوپ الکترونی عبوری (TEM) و خصوصیات مغناطیسی با استفاده از مغناطیس‌سنج ارتعاش نمونه (VSM) انجام شد. علاوه بر این، تحلیل عملکرد جذب، یعنی راندمان حذف رنگ و میزان تخریب، به عنوان جاذب مواد کاندید با استفاده از طیف‌سنجی UV-Vis انجام شد. تحلیل داده‌ها از ساختار و فاز rGO / Fe₃O₄، ساختار اسپینل مکعبی با اندازه‌ی بلوری ۳۸–۲۶ نانومتر را نشان می‌دهد. تحلیل گروه عملکردی وجود C- OH، O = C، C-O و Fe-O را نشان داد. بررسی میکروگرافی تصویر TEM نشان داد که اندازه‌ی ذرات نمونه در محدوده ۱۰ – ۳۰ نانومتر است. با پوسته‌ی ضخیم، مغناطش اشباع rGO / Fe₃O₄ از ۲۲.۶۰ به ۱۸.٤۸ emu / g کاهش یافته و از ۲۹.۲۱ به ۱۰.٤٥ emu / g برای Fe₃O₄ کاهش یافته است. سرانجام، ترکیب rGO بر دیواره‌ی پوسته تأثیر می‌گذارد به‌گونه‌ای که Fe₃O₄ را به عنوان هسته محصور می‌کند. جالب توجه این که با کاهش پوسته ویژگی جذب رنگ‌های طبیعی rGO / Fe₃O₄ افزایش یافته است.